Bulletin of Mathematical Biology, Vol. 58, No. 4, pp. 611–641, 1996
Elsevier Science Inc.

0092-8240/96 $15.00 + 0.00

0092-8240(96)00037-7

A STUDY OF THE BIFURCATION BEHAVIOUR OF A MODEL OF FLOW THROUGH A COLLAPSIBLE TUBE

■ J. P. ARMITSTEAD and C. D. BERTRAM
Graduate School of Biomedical Engineering,
University of New South Wales,
Sydney, Australia 2052

(*E.mail*: *jeffa,chrisb@gsbme.unsw.edu.au*)

■ O. E. JENSEN
Department of Applied Mathematics and Theoretical Physics,
University of Cambridge,
Cambridge, England CB3 9EW

(*E.mail*: *O.E.Jensen@damtp.cam.ac.uk*)

Most of the elastic tubes found in the mammalian body will collapse from a distended circular cross section and when collapsed may undergo flow-induced oscillations. A mathematical model describing fluid flow in a collapsible tube is analysed using the software package AUTO-86. AUTO-86 is used for continuation and bifurcation problems in systems of non-linear ordinary differential equations. The model is a third-order lumped-parameter type and is based on the classical "Starling resistor"; it describes the unsteady flow behaviour and, in particular, the experimentally observed self-excited oscillations, in a way which is simple enough to give physical understanding, yet still firmly based on fluid mechanical principles. Some of the bifurcation types found in this model bear close resemblance to the types suggested by experimental observations of self-excited oscillations in collapsible tubes; they thus shed some light on the various topological changes which occur in practice, particularly in view of the fact that some of the points found numerically are difficult to achieve experimentally, while the existence of others can only be inferred indirectly and uncertainly from experiment.

Introduction. Most organisms of over a few dozen cells have come to possess systems which incorporate some form of "conduit" for the distribution and collection of fluids and some means of eliciting bulk flow within the conduit. Examples of such systems within the human body include the cardiovascular system, the gastrointestinal system and the respiratory system (Guyton, 1986). In mammals these conduits take on the form of elastic tubes of nearly circular cross section when distended.

It is of considerable interest, both theoretically and practically, that under certain flow and external pressure conditions, most of the elastic

tubes found in the mammalian body will collapse from a distended circular cross section. Further, as a particular subset of this behaviour, tubes of this kind may undergo self-excited oscillations in which the cross section varies between an oval and a more complex double-chambered figure-eight shape (Conrad, 1969). Examples of both collapse and self-excited oscillations have been observed in the human body. In general, veins above the level of the heart are collapsed due to a normally negative transmural (inside minus outside) pressure. Other examples of simple collapse occur in the urethra during micturition and in the pulmonary airways (Shapiro, 1977). Examples of oscillations may include those in systemic arteries when a sufficiently negative transmural pressure is applied during clinical sphygmomanometry (Ur and Gordon, 1970). Other *in vivo* examples of oscillations include those in the veins near the heart (only occasionally recorded) (Matsuzaki, 1986), the collapse and oscillation of the specialised airways of the larynx during vocalisation, the similar oscillation of the avian syrinx during calling (King and McLelland, 1984) and forced expiratory wheezes (Grotberg and Gavriely, 1989).

Investigation of collapsible-tube behaviour. The interesting behaviour associated with flow in collapsible tubes has attracted many workers from various fields to study it both *in vivo* and, more typically, on the laboratory bench. Among the more recent investigations, both experimental (Bertram *et al.*, 1990, 1991) and theoretical (Bertram and Pedley, 1982; Cancelli and Pedley, 1985; Morgan and Parker, 1989), most have involved an experimental setup known as the Starling resistor (Knowlton and Starling, 1912).

The Starling resistor (see Fig. 1) has an elastic tube suspended in a controllable-pressure chamber between two rigid tubes. The upstream tube

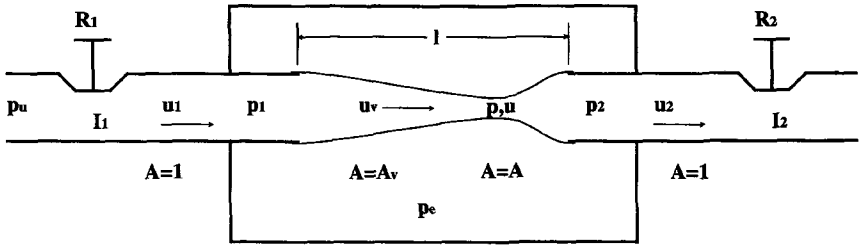

Figure 1. The collapsible tube or Starling resistor model. The collapsible section of the tube is enclosed in a sealed chamber at pressure p_e and fed from a constant pressure head upstream of p_u. Inlet and outlet conditions are determined by lumped parameters for resistance and inertance. Flow conditions within the collapsible tube are described by three ordinary differential equations for the independent dimensionless variables of upstream and downstream fluid velocity and the cross-sectional area at the point of maximum collapse (see Appendix for details).

is connected to an adjustable pressure head, and the flow characteristics can be modified by changing the inlet–outlet conditions.

Two distinctive properties characterise the flow behaviour of collapsible tubes: flow limitation and self-excited oscillation (Bertram *et al.*, 1991). Consider the Starling resistor in Fig. 1 with collapsible segment upstream pressure p_1, downstream pressure p_2 and chamber pressure p_e. Flow limitation occurs when the downstream transmural pressure $(p_2 - p_e)$ is negative, that is, chamber pressure is greater than the pressure in the downstream collapsible segment of the tube. If the upstream transmural pressure $(p_1 - p_e)$ is maintained constant, then it is found that flow rate through the tube is essentially independent of the driving pressure difference $(p_1 - p_2)$, and hence only depends on the upstream circuit conditions (Shapiro, 1977).

In the flow-limiting range of these negative downstream transmural pressures, self-excited oscillations can occur. A full understanding of the mechanism of these oscillations has yet to be achieved. More than one category of oscillations has been observed experimentally, and indeed Bertram *et al.* (1991) have identified more than six different classes of oscillations under different driving conditions.

Mathematical modelling of collapsible-tube behaviour. Complementing the experimental investigation of Starling-resistor-like setups has been a parallel attempt to examine collapsible-tube behaviour using purely mathematical models. These can generally be classified into two groups: lumped-parameter models, in which the flow is characterised by a number of time-varying spatially invariant parameters such as cross-sectional area at the point of collapse, and more complex models in which the selected parameters are considered to vary both temporally and over one or two spatial dimensions. The former models can be represented by sets of autonomous ordinary differential equations, while the latter models require sets of partial differential equations in order to account for both spatial and temporal variation. In both cases the equations are non-linear due to the associated fluid–mechanical principles. Partial differential equations are required in order to take into account wave propagation. It has been postulated (Kamm and Pedley, 1989) that super-critical flow (fluid speed greater than the propagation velocity of small-amplitude waves), which leads to "choking", may be a prime mechanism of unsteady flow in collapsible tubes.

Application of the AUTO-86 software package. The object of the work discussed here was to analyse a lumped-parameter model, studied by Bertram and Pedley (1982), using software called AUTO-86 which was

especially designed to be applied to bifurcation and continuation problems involving ordinary differential equations. The equations of Bertram and Pedley are derived in the Appendix, which also explains the non-dimensionalisation scheme. AUTO, developed by Doedel and Kernévez (1986), has the ability to trace out solution branches, both static and periodic, over a user-selected range of control space for sets of ordinary differential equations. It can also locate bifurcation points of the equilibria and flag them for subsequent tracing out of any new branch thence emanating. Finally, it can continue bifurcation points in two-parameter space. Thus, for example, the location of a Hopf bifurcation point can be traced out for two independent variables. The independent variables investigated in this study were upstream pressure p_u and chamber pressure p_e. A new version, AUTO-94, is now available.

Methods. AUTO was run on an Apollo DN3000 work station. Hard copy of graphics was obtained using programs supplied with AUTO linked to in-house graphics routines and various Postscript translation tools. Initial model conditions were obtained from a fourth-order Runge–Kutta algorithm with adaptive step-size control. The Runge–Kutta integrator was also used independently, proving useful in the investigation of control space which AUTO could not be made to negotiate.

The algorithms used by AUTO are described in some detail in the reference manual (Doedel and Kernévez, 1986). AUTO is capable of solving numerically a system of ordinary differential equations (at discrete intervals) as a free parameter is varied for both steady and unsteady solutions. Stability is tracked and bifurcation points are detected by monitoring the linearised Jacobian, in the case of steady solutions, and Floquet multipliers (a numerical equivalent of the Poincaré multiplier), in the case of unsteady solutions.

Results.

Chamber pressure p_e as the control parameter. At low values of p_e the model tube is wide open and constant flow conditions are established. Figure 2 shows a bifurcation diagram with chamber pressure p_e as the control-space parameter, $p_u = 295$. The ordinate is A, the non-dimensional area at the most collapsed part of the tube, or in the case of unsteady behaviour, the maximum of $A(t)$. Stable, steady solutions are indicated by full lines; unstable, steady solutions by dotted lines. Filled circles represent the path of a stable, unsteady solution; open circles that of an unstable, unsteady solution (e.g. Figure 6). Three bifurcation points are indicated on Figure 2. A pair of folds or saddle-node bifurcations (marked by open squares) are associated with the hysteretic collapse of the tube as p_e is

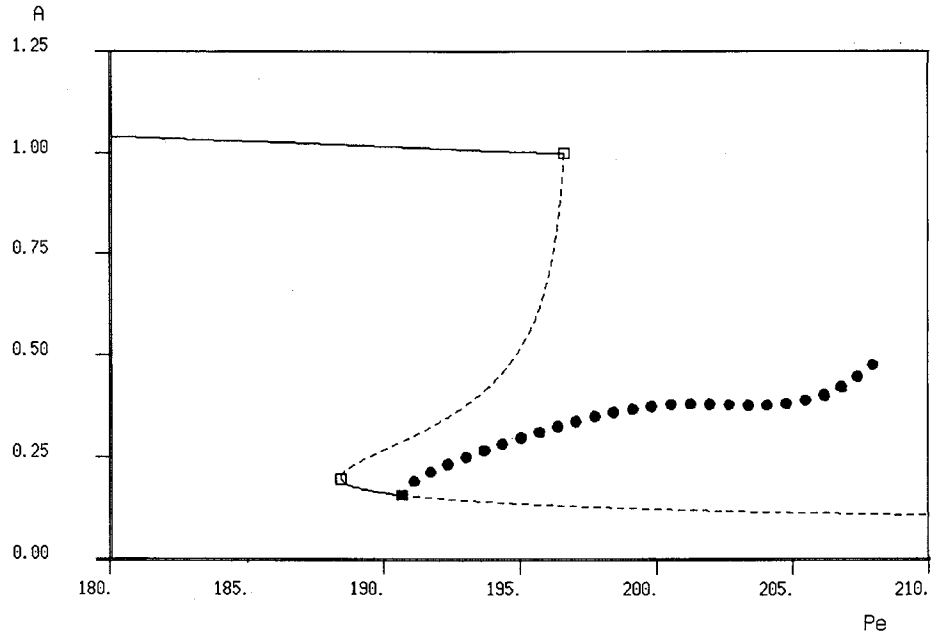

Figure 2. A bifurcation diagram in (p_e, A) space for $p_u = 295$, which shows the topological changes in the model solutions as the control parameter p_e is varied. The control parameter is measured on the horizontal axis, while the ordinate denotes the maximum value of the dimensionless variable A, the area of the most collapsed section of the tube. Solid lines represent stable steady solutions, broken lines represent unstable steady solutions, and filled circles represent stable unsteady solutions (limit cycles). Bifurcations, or points at which equilibria change topologically, are represented by symbols. This figure shows a pair of folds (marked by open squares) and a Hopf bifurcation (marked by a filled square) at which a path of limit cycles is born. Note that the slope discontinuity at $A = 1$ in this and subsequent figures is a consequence of the way the tube law is formulated in equation (A13).

increased. Following along a steady solution branch, each fold marks the transition of a single purely real eigenvalue from the negative domain to the positive as stability is lost. It should be noted that during the analysis of the model (which consists of three coupled ordinary differential equations), at least one purely real and strictly negative eigenvalue was always found; this is consistent with our numerical findings that the dynamics are constrained to that which can be represented in a two-dimensional phase space. The filled square at $p_e \approx 191$ denotes a Hopf bifurcation where stability is lost via the movement of a complex conjugate pair of eigenvalues across the imaginary axis into the positive quadrants. A repellor is thus created and limit cycles subsequently develop. Each of the bifurcation points can be continued in two-parameter (p_u, p_e) space. To the right of Fig. 2 it can be seen that the limit cycles increase in amplitude, and eventually become unstable at p_e values beyond those shown.

Upstream pressure p_u as the control parameter. Figure 3 shows a bifurcation diagram in (p_u, A) space. At low p_u values the tube is completely collapsed, steady flow is established and A increases slowly with p_u. A Hopf bifurcation again indicates the birth of limit cycles at the critical p_u value of approximately 140. For this particular value of p_e (200) the solution path of limit cycles emanating from the Hopf bifurcation disappears at a type of homoclinic connection called a blue-sky catastrophe (Thompson and Stewart, 1986) at $p_u \approx 305$. A homoclinic connection in general is "a trajectory that approaches the same equilibrium (necessarily a saddle) for $t \to -\infty$ and for $t \to +\infty$" (Thompson and Stewart, 1986). The tube reopening is again associated with a pair of folds, although the lower one is qualitatively different from that in Fig. 2 because it marks the

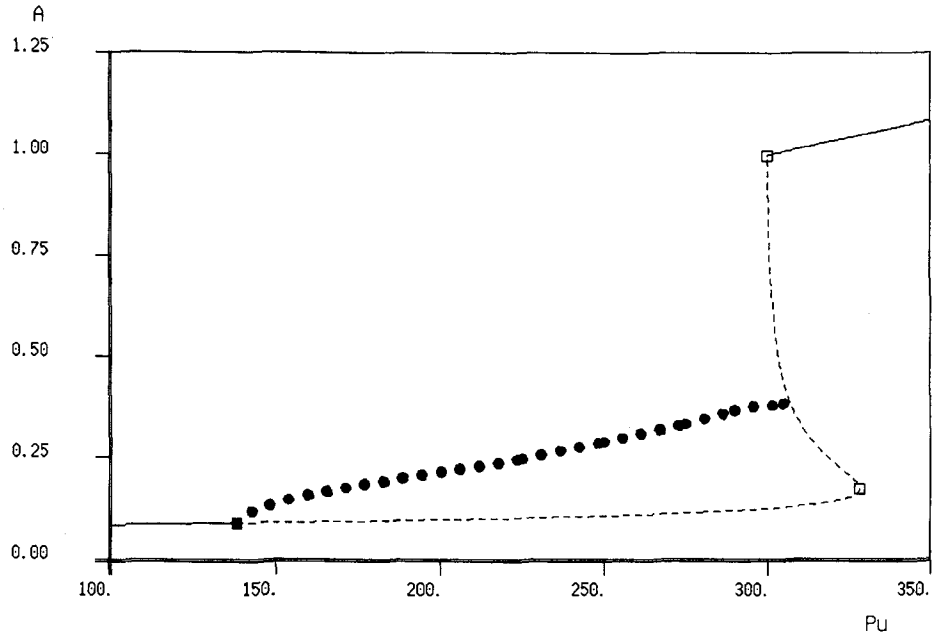

Figure 3. A bifurcation diagram in (p_u, A) space for $p_e = 200$. Lines again represent solution paths and symbols represent bifurcation points (see Fig. 2). The stable steady solution path at the left of the diagram is broken by a Hopf bifurcation and two fold bifurcations before reappearing to the right of the diagram. A path of limit cycles is born at the Hopf bifurcation and proceeds to the right before disappearing at a homoclinic connection (where the path of filled circles meets the dashed curve) at $p_u \approx 305$. As p_u is increased toward the connection, the period of the limit cycles increases and eventually tends to infinity at the connection point itself. Any slight jump across the connection results in the disappearance of the limit cycles altogether. (Note that a second path of limit cycles exists in this region of control space but is not shown here. See Fig. 11, panel VII.)

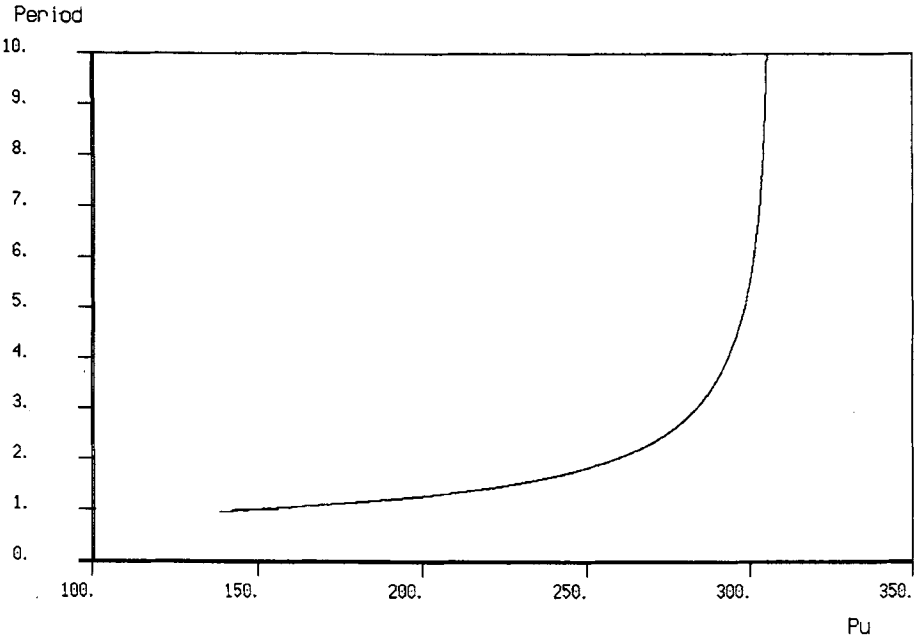

Figure 4. A plot of p_u versus limit-cycle period for $p_e = 200$ as the homoclinic connection shown in Fig. 3 is approached. The period tends to infinity at the homoclinic connection point.

transition between two different *unstable*, steady solution paths. Figure 4 shows the period of the limit cycles plotted against p_u. As the homoclinic connection is approached, the period rises steeply toward infinity.

Figure 5 shows two phase-plane plots in (u_2, A) space at $(p_u, p_e) = (320, 200)$, close to the lower fold. Both orbits are captured by the upper stable solution (tube open), but they proceed by different routes. The lower starting point spirals out from a repellor before entering the basin of attraction of the stable solution, while the upper orbit proceeds more directly, albeit constrained by the flow associated with the lower orbit.

Low p_u values with p_e as control parameter. At lower p_u values the tube collapses non-hysteretically (i.e. no folds) as chamber pressure p_e is increased. Figure 6 shows a bifurcation diagram in (p_e, A) space for $p_u = 25$. A Hopf bifurcation again marks the start of a path of limit cycles at $p_e \approx 380$, but the fate of this solution path is markedly different. At around $p_e = 530$ a cyclic fold (analogous to a fold for equilibria, as met above, but for limit cycles) is encountered where an unstable and a stable solution path meet and annihilate each other. The solution path of unstable limit

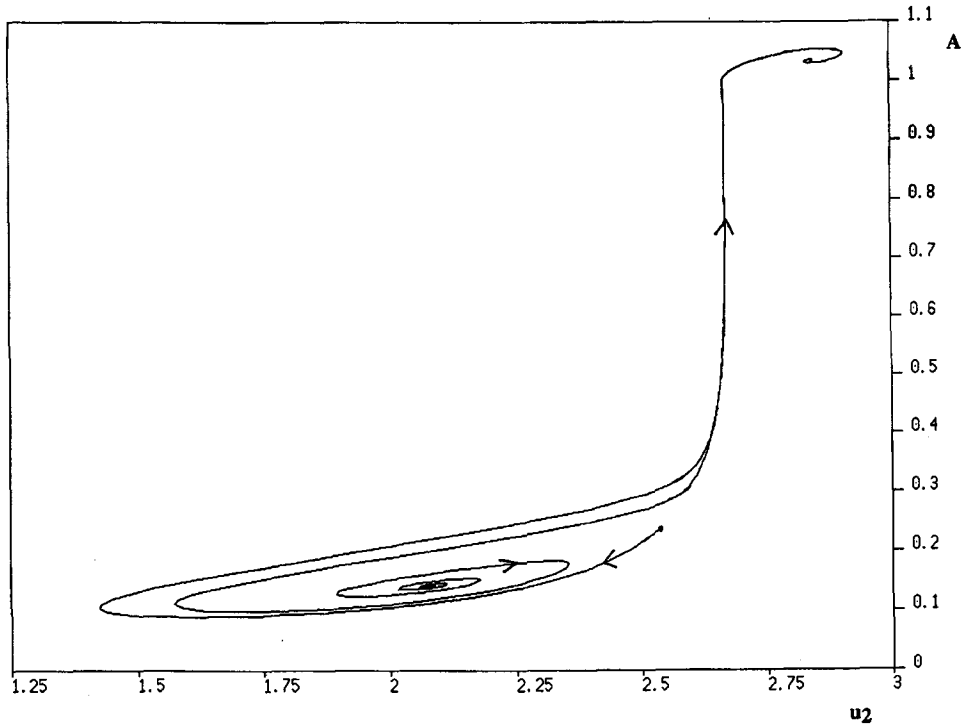

Figure 5. A (u_2, A) phase-plane plot of two integrations forward in time for $p_u = 320$ and $p_e = 200$. The starting points for the two runs are the two points on Fig. 3 where a vertical line at $p_u = 320$ (not drawn) would intersect the dashed curves for unstable steady equilibria. The first integration (originating near $u_2 = 2.1$) starts from the lower unstable equilibrium (repellor) curve of Fig. 3; the second (originating near $u_2 = 2.55$) starts from the upper unstable equilibrium curve (saddle). Both solutions are captured by the upper (tube open) stable equilibrium point, although the trajectories they follow to get there are qualitatively different. Both equilibrium points have associated with them one eigenvalue out of three which is purely real and negative; the other two eigenvalues are, in the first case, a complex conjugate pair with positive real parts describing a repellor and, in the second case, two purely real and positive eigenvalues describing a saddle. These eigenvalues only describe behaviour local to the equilibrium point, not the ultimate capture by the solution at $A > 1$. Thus the repellor trajectory initially spirals out before being captured, while that of the saddle does not. The saddle trajectory is, however, additionally forced to curve around the repellor once away from the local environment of its equilibrium point.

cycles proceeds to the left and expands indefinitely at around $p_e = 200$. For $p_e > 530$ there is thus apparently no stable solution, a physically unlikely scenario. The full likely topology of the situation is postulated below.

Two-parameter continuation in (p_u, p_e) space. Each of the bifurcation points shown so far—the fold, the Hopf bifurcation, the cyclic fold and the

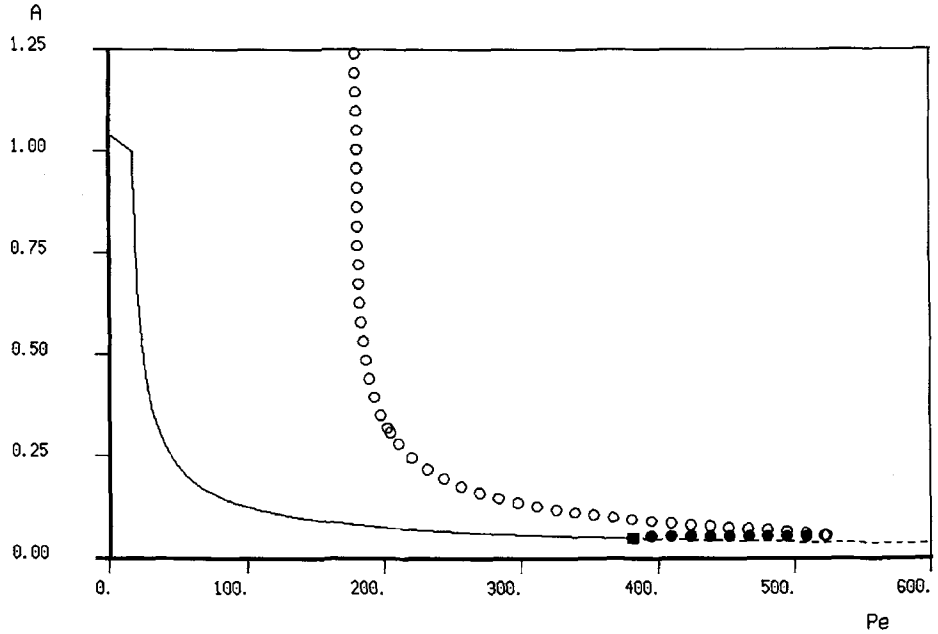

Figure 6. A bifurcation diagram in (p_e, A) space for $p_u = 25$. As the control parameter p_e is increased, the stable steady solution to the left of the diagram rapidly falls to a markedly lower A value, but not through a fold bifurcation. At no p_e value in this region is there an instability. Two types of unsteady solution paths are shown in this diagram: a stable path marked by filled circles and an unstable path marked by open circles. As p_e is increased to the right of the diagram, the two unsteady solution paths meet and are annihilated (cyclic-fold bifurcation). To the right of this bifurcation all trajectories leave the neighbourhood, i.e. there is no local stable solution. (Note that a second path of stable limit cycles exists in this region of control space, but was too steep to be detected. See Fig. 9, panel B.)

homoclinic connection—was continued in two-parameter (p_u, p_e) space. (The homoclinic connection is traced out by considering a limit cycle of very large fixed period as being an approximation to an orbit of infinite period.) This is most instructive in determining the overall dynamical behaviour of the model as p_u and p_e are varied. For example, the two-parameter continuation of homoclinic connections suggested that the curve was double-valued in p_e. Figure 7, with $p_u = 306$, shows this to be the case. Two homoclinic connections are shown in (p_e, A) space at $p_e \approx 196$ and 198. The unsteady solution path at $p_e > 198$ was traced out "manually" using the Runge–Kutta algorithm.

Figure 8 shows a composite of all two-parameter continuation loci. The diagram has been divided up into segments, each having a specific topology, by vertical lines at values of p_u corresponding to critical points. The latter

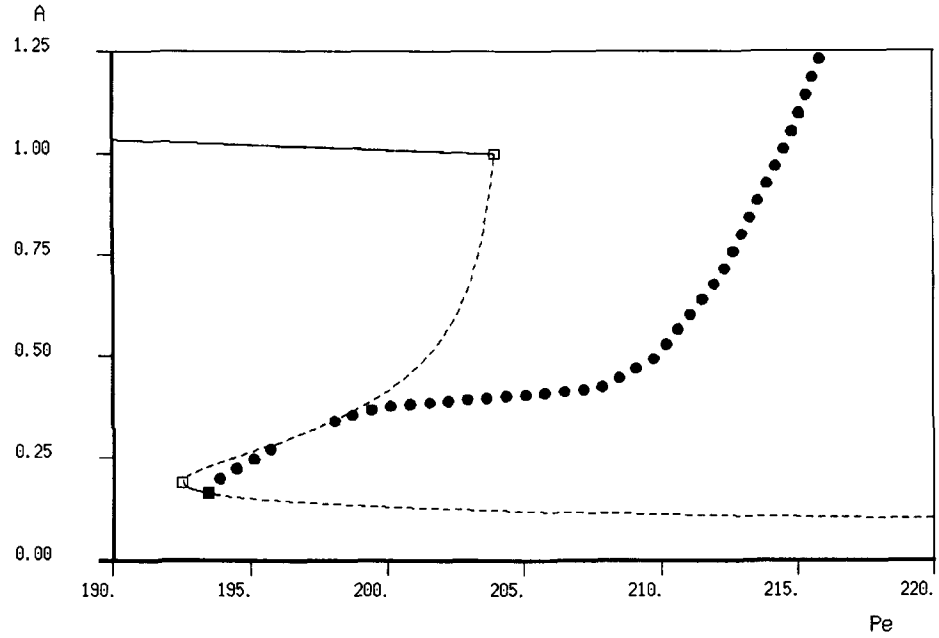

Figure 7. A bifurcation diagram in (p_e, A) space for $p_u = 306$ containing two fold bifurcations, a Hopf bifurcation and two homoclinic connections. The path of steady limit cycles born at the Hopf bifurcation is "split" by the homoclinic connections before continuing its march to the right. As p_e is increased, the limit cycles eventually attain maxima greater than the value of the stable (tube open) solution at the left of the diagram.

mark qualitative transitions in the one-parameter bifurcation diagrams considered so far. Diagrammatically, each line marks a curve intersection point or a curve maximum or minimum. In this diagram, the curves marked f_1, f_2 represent the fold loci, H the Hopf locus, cf_1, cf_2 the cyclic-fold loci and hc_1, hc_2 the homoclinic loci. The regions are labelled from A to K (excluding I for the sake of clarity); schematic bifurcation diagrams representative of the regions are shown in Fig. 9. Each of these schematic representations was sketched after considering a "slice" through the middle of the region and combining the result with general knowledge of the bifurcation behaviour of the model obtained from the various AUTO runs performed. Figure 10 shows the same composite diagram now dissected into regions of p_e; Fig. 11 contains schematic representations of the (p_u, A)-space bifurcation diagram in each region.

Discussion. The analysis of the tube model demonstrated a variety of flow behaviours associated with a number of modalities of stability loss. Both

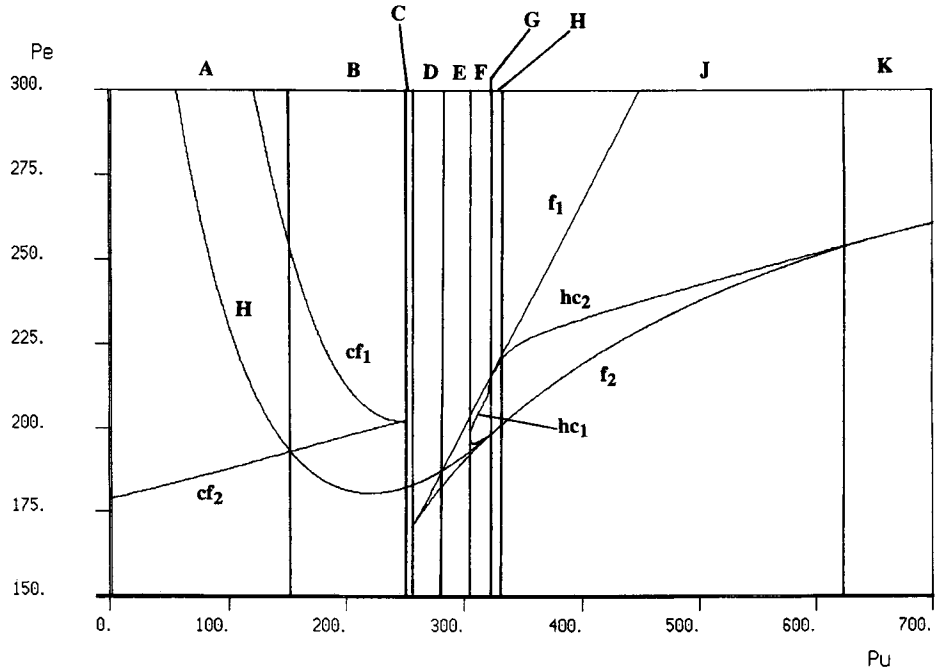

Figure 8. The composite two-dimensional bifurcation diagram sectioned into different regions A–K bounded by values of p_u at which topological changes in the model occur. A slice through any region results in a topologically distinct one-dimensional bifurcation diagram with control parameter p_e. Curve identifiers: H, Hopf; f, fold; cf, cyclic fold; hc, homoclinic connection.

local bifurcations (Hopf, fold, cyclic fold) and a global bifurcation (homoclinic connection) were identified. Global bifurcations are characterised by large-scale changes in phase-space flow and subsequent changes in the basins of attraction of equilibria. Local bifurcations, by contrast, do not affect the flow in phase space far from the site of the bifurcating equilibria; they are mathematically characterised by fundamental changes in the eigenvalues of the linearised Jacobian, in the case of steady equilibria, and changes in the Poincaré multipliers, in the case of limit cycles. Global bifurcations such as homoclinic connections do not involve changes in these characteristic components; rather, they involve changes in the topological configuration.

The only local bifurcation of unsteady equilibria identified—the cyclic fold—was a co-dimension-1 bifurcation (i.e. obtained through variation of one control parameter) in which one Poincaré multiplier crosses the unit circle. Phase-plane analysis of the stable and unstable limit cycles associated with the cyclic fold failed to find any "spiralling" orbits approaching

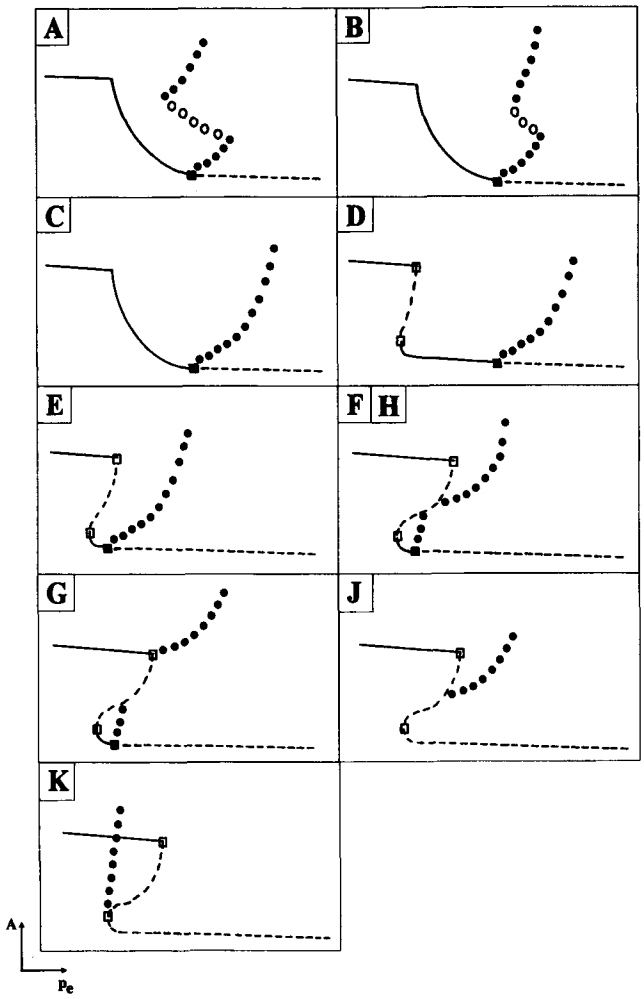

Figure 9. Sketches of the topologically distinct one-dimensional bifurcation diagrams representative of each region delineated in Fig. 8. The control parameter for each is p_e and the ordinate again denotes the maximum value of the dimensionless variable A. The sketches are arrived at by considering that there must be a topologically smooth transition from each region to adjoining ones. Symbols correspond to those in the diagrams generated by the continuation software (e.g. Figs. 2 and 3). Note that homoclinic connections are not marked with a special symbol, but occur where stable oscillatory paths (filled circles) meet unstable steady paths (dashed curves), in panels F–K.

the limit cycles and no evidence was found of bifurcation to an invariant torus either by phase-plane analysis or as flagged by AUTO. In fact, the model dynamics were found to be constrained to a two-dimensional centre manifold; i.e. the phase portrait is generally organised by those eigenvalues with zero real parts. As stated previously, in the analysis of this third-order

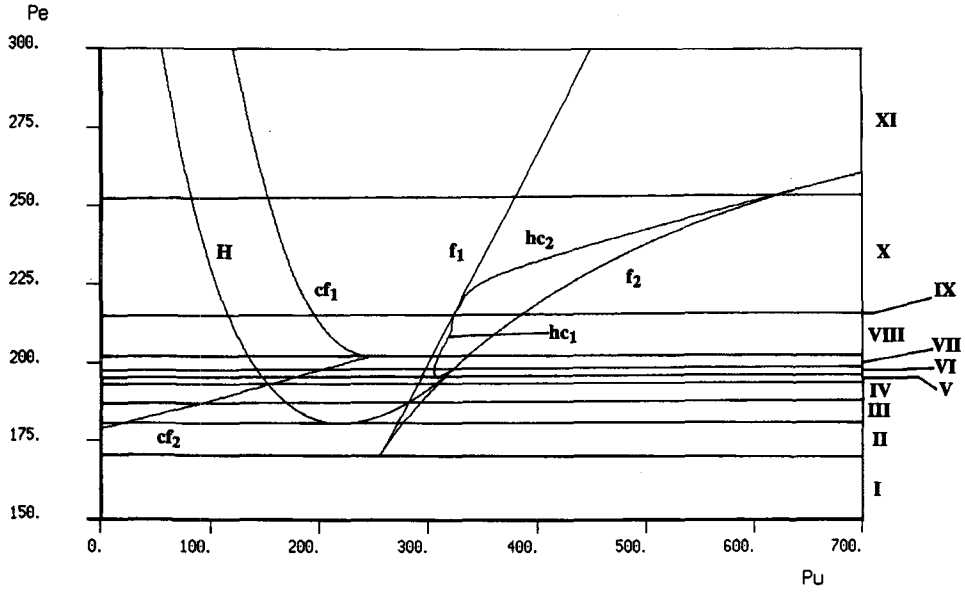

Figure 10. The composite two-dimensional bifurcation diagram of Fig. 8, this time sectioned into regions I–XI bounded by topologically critical values of p_e. A slice through any region now results in a topologically distinct bifurcation diagram with control parameter p_u.

model one purely real and negative eigenvalue was always observed, and so the interesting flow in phase space always reduced to two dimensions.

Any dynamical system constrained to a two-dimensional, planar centre manifold can be expected to display only simple limit cycles. No evidence was found of higher-dimensional attractors that would represent, for example, quasi-periodic or mode-locked interactions of distinct oscillations or dynamical chaos.

A further important observation regarding the model was that the homoclinic connection found was not transverse. A transverse homoclinic connection requires that the dimension of its stable manifold (containing the part of the orbit approaching the saddle) and the dimension of its unstable manifold (containing the part of the orbit leaving the saddle) sum to a value greater than the dimension of phase space. Careful inspection of the homoclinic connection revealed a maximum sum of dimensions of only 3. Transverse homoclinic connections have been identified as key features of systems containing regions of chaotic behaviour, and they can lead to complex structures such as homoclinic tangles (Abraham and Shaw, 1984; Guckenheimer and Holmes, 1986). The lack of any transverse homoclinic connection in this model analysis and the fact that the dynamics are

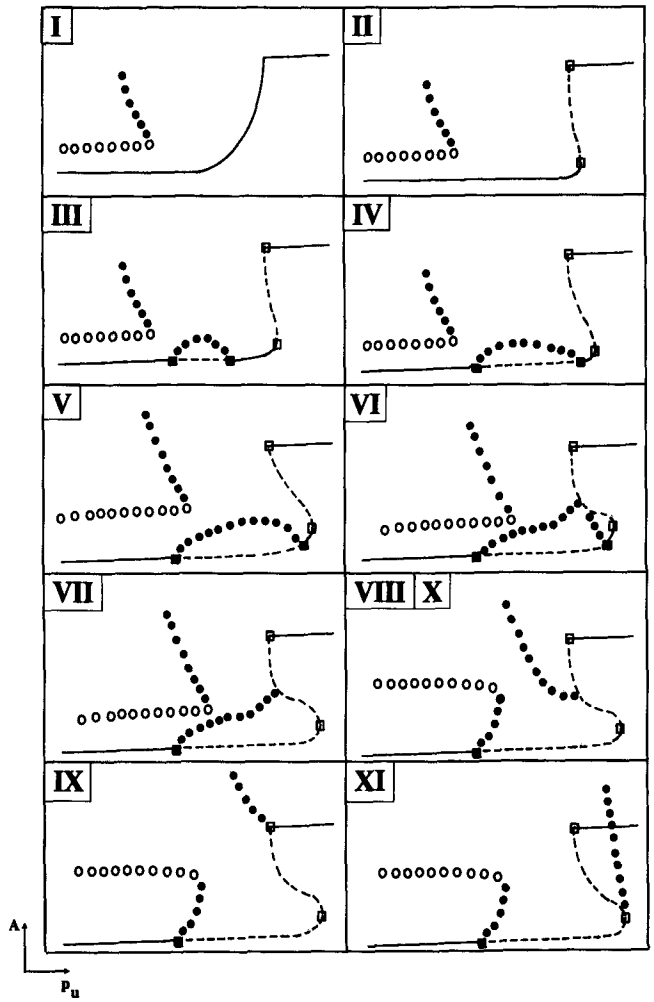

Figure 11. Sketches representative of the bifurcation diagrams in each region delineated in Fig. 10. The control parameter for each diagram in this case is p_u, while the ordinate again represents A.

constrained to a centre manifold of dimension 2, have implications for the types of behaviour observed and would certainly preclude any dynamical chaos.

Behaviour in regions of (p_u, p_e) *space delimited by* p_u *value.* The two-parameter composite bifurcation diagram can now be explained in terms of changes in bifurcation behaviour. The first stage in this process is the

identification of critical points, which delineate different regions of the diagram. Such points include the intersection of different loci of bifurcation points and geometrical maxima and minima of locus curves with respect to the control parameters. The intersections of bifurcation loci are also known as co-dimension-2 points, which can only be reached by adjusting both of the control parameters, p_u and p_e, simultaneously. The critical points were shown in Fig. 8 along with lines which sectioned the diagram into different regions of p_u and passed through these points.

Consider Figs. 8 and 9 in detail. Starting at the far left of the two-parameter diagram with a low value of p_u, region A has three bifurcation points: a Hopf bifurcation and two cyclic-fold points. As p_u is increased and region B is entered, the cyclic fold with larger A value moves to a position in p_e to the right of the Hopf bifurcation. On entering region C, the vertex of the cyclic-fold locus has been passed, and hence the cyclic folds have moved together and disappeared. While p_u is increased, the gradient associated with the collapse of the tube in the bifurcation diagram is getting steeper, and finally a pair of folds (saddle-node bifurcations) is introduced at the beginning of region D.

There is now hysteresis involved in the steady solution path because of these folds, which steadily separate with increasing p_u. As p_u is increased further, the Hopf bifurcation marches leftward in the bifurcation diagram until it reaches a point where it is between the folds in terms of p_e, as seen in region E. Region F shows the emergence of two homoclinic connections in the unsteady solution path. This occurrence is brought on by two factors. First, the unsteady solution path is steepening with increasing p_u, bringing it closer to the unstable steady solution path. Second, the two folds are separating and the Hopf bifurcation is also moving back toward the lower fold. This results in the unsteady solution path touching the saddle path, creating a single homoclinic connection from which two unsteady solution paths emanate. This situation exists only on the boundary between region E and region F. Inside region F the homoclinic connection has become two.

Following the upper branch of the locus of homoclinic points in region F in Fig. 8, it can be seen that it approaches the upper fold locus. One of two scenarios is then possible: either (a) the two curves meet and a bifurcation occurs or (b) the two curves do not touch and no bifurcation exists. As discussed below, fundamental differences were found in the homoclinic connections on either side of this postulated meeting point, thus indicating scenario (a). Therefore the homoclinic locus just touches the upper fold locus at one point (situation G) before receding. This is consistent with the homoclinic connection running up the unstable steady solution to the top fold, beyond which it cannot proceed. Thus the bifurcation diagram for region H is identical to that for region F.

The co-dimension-2 point which turns region H into region J is particularly interesting because it involves the intersection of the lower fold and Hopf and homoclinic loci. (The two-parameter diagram does not show this intersection precisely because AUTO was unable to advance the approximate homoclinic locus far enough. The location of the point itself was determined as the intersection of the fold locus with the endpoint of the Hopf locus at $(p_u, p_e) \approx (328, 200)$.) In terms of the bifurcation diagram (Fig. 9) this results in the convergence of the two ends of the lower unsteady solution path at the lower fold point, and hence the disappearance of this branch. This leaves only the upper branch emanating from the other homoclinic connection as shown in region J. Region H reflects the situation before this happens, with the upper homoclinic branch having receded from the upper fold point and the lower homoclinic branch still extant; hence, region H has qualitatively the same bifurcation diagram as region F.

If the homoclinic locus is followed further into region J, the unsteady solution path becomes extremely steep, with the homoclinic connection continuing to move toward the lower fold on the bifurcation diagram. This is evident at the right-hand end of Fig. 8, where the fold and homoclinic loci appear to coalesce or, perhaps, even cross at the start of region K. Topological consistency would ordinarily demand the creation of a new locus of Hopf bifurcations at such a meeting point, but no evidence of this was found. Inspection of the relevant data files revealed that as far out as at $p_u = 780$ the two curves differ in p_e value only at the fourth decimal place. This suggests that, in fact, the two true loci neither cross nor coalesce, in which case there is no region K.

The sketches in Fig. 9 reflect the amplitude of oscillations as found by the continuation software. The result is that the paths of stable oscillatory solutions in many cases climb rapidly out of the top of the diagram, leaving a region on the right-hand side where apparently no stable solution exists. Experimentally, one would expect a high value of p_e to lead to the eventual abolition of oscillations. Dynamically, it is believed that a stable solution should exist, implying that at some extremely high A value the stable oscillatory path eventually lies over the "uncovered" unstable steady path.

Behaviour in regions of (p_u, p_e) *space delimited by* p_e *value.* Considering now Figs. 10 and 11. Beginning at a low value of p_e, the only locus crossed by a slice in p_u is the cyclic-fold line. Thus, the only bifurcation point is a cyclic fold and the tube opens non-hysteretically as shown in region I. At increased p_e the vertex of the fold locus is crossed and two folds appear in the steady solution path in region II. The cyclic fold moves toward the right of the bifurcation diagram.

With little further increase in p_e, the minimum of the Hopf bifurcation locus is passed and two Hopf bifurcation points are born, as seen in region III. These two points are joined by a single unsteady solution branch, which, in the beginning, is quite shallow. As p_e is increased further, the unsteady solution path "inflates", the Hopf bifurcation points move further apart and eventually the right-hand Hopf moves between the folds as seen in region IV.

While this has been happening, the cyclic fold has continued to move to the right of the bifurcation diagram, until it in fact passes the left-hand Hopf bifurcation at the beginning of region V. The value of p_e at which this happens corresponds to the intersection of the Hopf and cyclic-fold loci in Fig. 10. There are now two limit cycles which exist for a single value of p_u, and an unstable limit cycle. This unstable limit cycle is the separatrix between the basins of attraction of the two stable limit cycles.

Region VI begins at the lowest point (in terms of p_e) of the homoclinic locus, which, since the gradient of the curve with respect to p_e at that point is approximately zero, is assumed to be a minimum. The homoclinic locus is indeed double-valued in p_e, since the curve attains a positive gradient before terminating at the Hopf-saddle-homoclinic collision point. This point was determined as the endpoint of the Hopf locus, which is contained in the fold locus and has a p_e ordinate greater than the minimum in the homoclinic locus. Topologically this means that the Hopf-terminated unsteady solution path has inflated to the point where it has touched the unstable branch of the steady solution path. At this single value of p_e both of the unsteady paths emanating from the Hopf bifurcations terminate at the one homoclinic connection. As p_e is increased further, the two paths separate and two homoclinic connections result.

The Hopf-saddle-homoclinic collision marks the beginning of region VII. The right-hand homoclinic connection has disappeared at the collision, as has the right-hand Hopf bifurcation and its associated path of limit cycles. This leaves a single branch of limit cycles beginning at a Hopf bifurcation. The right end of this branch now begins to climb the unstable steady solution path with increasing p_e, bringing the two remaining unsteady solution paths closer together; they finally meet at the beginning of region VIII, at the cusp of the cyclic-fold locus on Fig. 10, resulting in an interchange of solution branches.

After this collision, the cyclic fold begins to recede to the left and the homoclinic connection again moves up toward the upper fold bifurcation. Region (or line) IX represents the single value of p_e at which the homoclinic connection co-resides with the upper fold point. The homoclinic bifurcation point then recedes from the fold locus and the bifurcation diagram (region X) again looks like region VIII. The unsteady solution

branch emanating from the homoclinic connection is now extremely steep, as alluded to previously. Finally, region XI corresponds to region K as discussed above.

Topologies of the (p_u, p_e)*-space diagram.* Now that the (p_u, p_e)-space diagram has been examined in terms of the logical progression through the various bifurcation diagrams described, the regions of different topological behaviour of the equilibria can be determined. Figure 12 shows the different regions of topological behaviour of the model and Fig. 13 shows sketches of the topological behaviour representative of each region. The sketch for the topology of the homoclinic connection is a special case in that it does not represent behaviour in a two-dimensional region of the two-parameter diagram; rather, this topology only exists for any point lying exactly on the homoclinic locus (remembering that the homoclinic locus, as plotted by AUTO, is an approximation to the true homoclinic locus).

These sketches can only represent the behaviour of the model in the local neighbourhood of the various equilibria. The exact basin of attraction

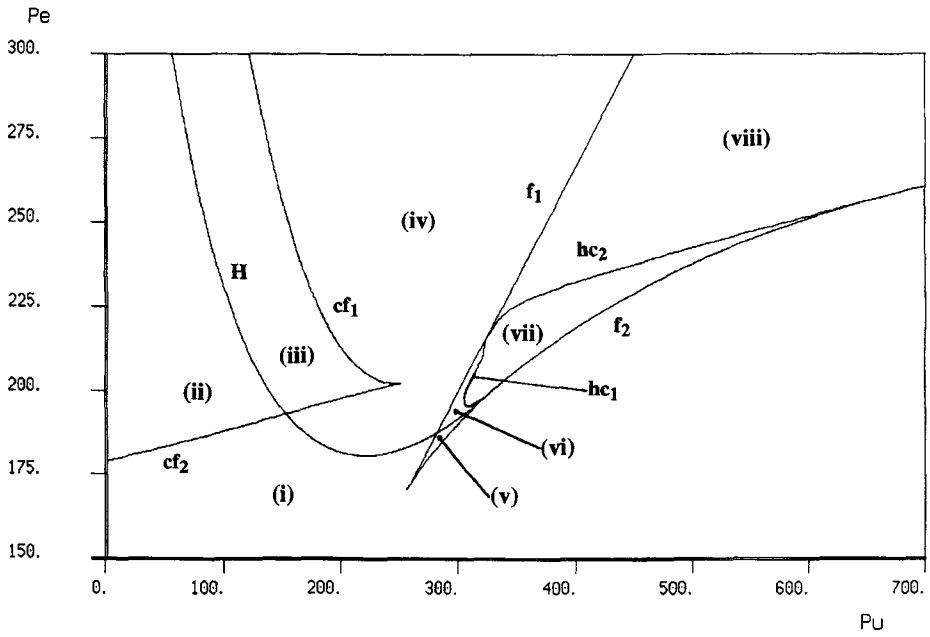

Figure 12. The composite two-dimensional bifurcation diagram, or control-space diagram, shown with the different areas of topological behaviour marked with lowercase roman numerals. Each area is bounded by the loci of bifurcation points. Each corresponds to a qualitatively distinct flow in phase space; see Fig. 13.

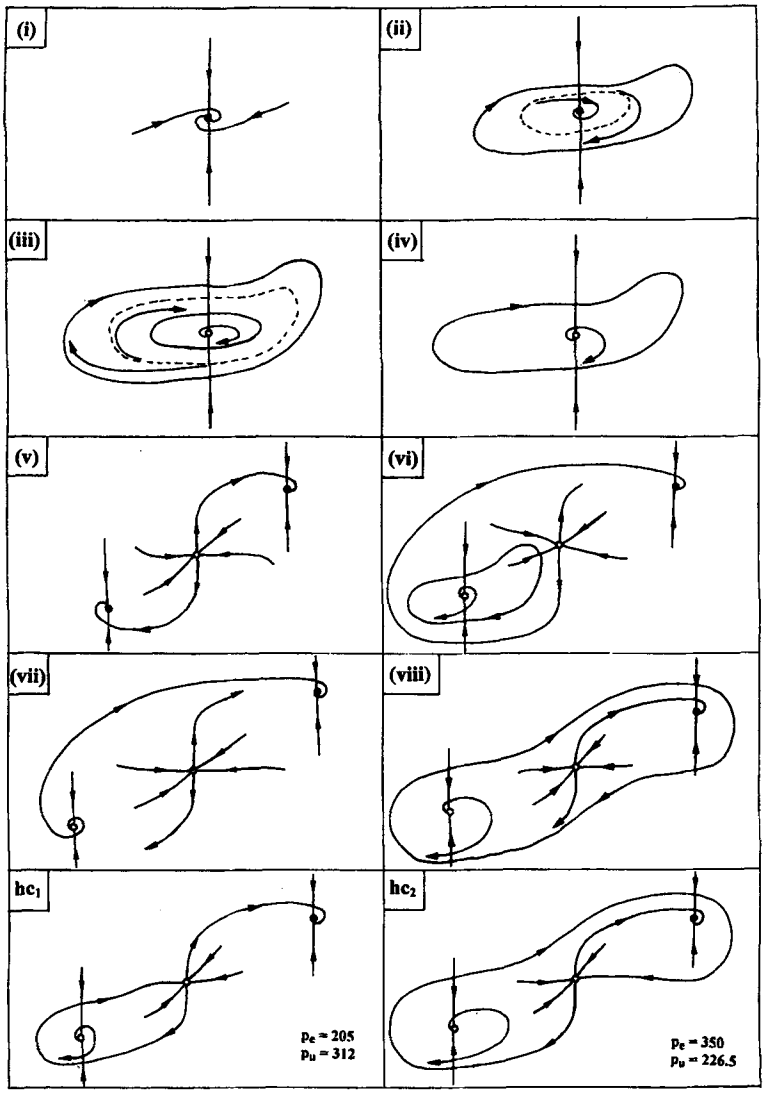

Figure 13. The different equilibria in two-dimensional control space, as marked in Fig. 12, shown sketched in phase space with their associated flows. Filled circles denote stable steady solutions (foci); open circles denote unstable ones (saddles). Dashed lines show unstable limit cycles, which are also sections through separatrices.

for each equilibrium could only be determined after rigorous phase-plane analysis. What can be determined here is the nature of the flow around the equilibria and the separatrices which might be expected for a consistent phase-plane diagram.

Region (i) represents the simplest behaviour the model exhibits, where all solutions converge to a single, stable equilibrium point. Since two of the eigenvalues associated with this point (at all equilibria of this type investigated) are part of an imaginary pair, its three-dimensional inset is as shown in Fig. 13. This depiction is consistent with the spiralling seen around this point (wherever investigated) and it can be characterised as a focus rather than a node and as an attractor of index zero. (Note that the index of a characteristic point is the name given to the dimension of its "outset". Attractors have only insets, saddle points have insets and outsets and repellors have only outsets.)

As region (ii) is entered the cyclic-fold locus is crossed, and a stable and an unstable limit cycle are simultaneously born. Further into region (ii) these limit cycles have separated: the unstable limit cycle becomes a separatrix between the stable point and the stable limit cycle. Although these limit cycles are three dimensional, they can be treated as two dimensional insofar as concerns their interactions with characteristic points and other limit cycles. Nevertheless, an attempt has been made in Fig. 13 to indicate the three-dimensional curvature and relative placement of the critical points in a way which is consistent with Fig. 12.

In order to move into region (iii), the Hopf locus must be crossed. This results in the stable point becoming unstable due to the crossing of the imaginary axis by a complex pair of eigenvalues associated with the point. The stable focus is thus replaced by an unstable focus (a repellor) and a stable limit cycle which grows out from the point of its birth. The phase plane as sketched in Fig. 13 now contains three limit cycles; the unstable limit cycle acts as a separatrix between the two stable ones. The view is again two dimensional and may be considered a cross section through a three-dimensional tubular separatrix.

Moving into region (iv) from region (iii), the cyclic-fold locus is crossed for a second time. This results in the annihilation of the inner two limit cycles as they move toward coincidence. This then leaves the unstable focus as the only characteristic point and the outer limit cycle as the only attractor.

In order to reach region (v), it is first necessary to recross the Hopf locus, thus returning to region (i). This results in the limit cycle shrinking into the unstable focus until it disappears, and the focus again becomes a stable equilibrium point. On now entering region (v) the fold locus is crossed and, for the first time, more than one characteristic point is extant. As the fold occurs, two new characteristic points are born: one is stable; the other unstable. The points are shown sketched with their associated insets and outsets in Fig. 13. The two stable points are foci of the same type, while the unstable point is a saddle of index 1. (Either one of the stable equilibrium

points can be annihilated with the saddle, corresponding to the two branches of the fold locus.)

The stable equilibrium points always have associated with them a complex pair of eigenvalues; in other words, they are always "focal" in nature rather than "nodal". This means that at a fold bifurcation, two of the eigenvalues must always be coincident at the origin of the eigenvalue plane, while the other is confined to the negative real domain. The two coincident eigenvalues then separate in one of three ways corresponding to three different equilibrium points: (1) the eigenvalues split into a complex pair with positive real parts (unstable focus or saddle of index 2); (2) one eigenvalue moves along the real axis in a positive direction, the other in a negative direction (saddle of index 1); (3) the eigenvalues split into a complex pair with negative real parts (stable focus or attractor, of index 0). All three outcomes are seen in region (vi): from left to right the critical points are a saddle of index 2, a saddle of index 1 and an attractor.

As region (vi) is entered, the Hopf locus is yet again recrossed, resulting in the birth of another limit cycle from the "lower" focus. The unstable focus which the limit cycle now surrounds is an index-2 saddle. This is consistent with the phase-plane results obtained by numerical integration, but again the exact nature of the whole three-dimensional phase space is not known. The insets of the middle saddle now form separatrices dividing the flow between the upper stable focus and the limit cycle.

Region (vii) is reached by crossing the (approximate) locus of the homoclinic connection. The limit cycle disappears via a "blue-sky catastrophe" (Thompson and Stewart, 1986), leaving just the three characteristic points. This situation is similar to that of region (v), except that the lower characteristic point is an unstable focus rather than a stable one. All solutions will now converge to the one stable equilibrium. A sketch (hc1) is included in Fig. 13 to show the situation which occurs exactly at the homoclinic connection. An inset and outset of the saddle are connected via an orbit of infinite period which encloses the unstable focus.

If the homoclinic locus is again crossed, a new region (viii) is entered, which, although separate from region (vi), is identical to it in terms of the equilibria present. The main difference between these two regions is in the behaviour of the limit cycle, which will be looked at in more detail below. The remaining panels in Fig. 13 will be discussed in this context.

The far right of the (p_u, p_e)*-space diagram.* At the far right of the (p_u, p_e)-space diagram (Fig. 8), the homoclinic locus and the f_2 branch of the fold locus appear to coalesce. While trying to determine the exact location of the homoclinic connection, limit cycles were studied in region

(viii) of Fig. 12 very close to the connection itself, to the right of (p_u, p_e) space. This area of the two-parameter diagram contains equilibria equivalent to those of region (vi) (a stable focus, a saddle and a repellor surrounded by a limit cycle) and spans the region J–region K boundary at which the fold locus and the homoclinic locus begin to be indistinguishable. These region-(viii) limit cycles have a large maximum value which exceeds the dimensionless throat-area value for the stable steady solution of approximately 1. Thus, if the AUTO convention of plotting unsteady solution paths on bifurcation diagrams with their maximum value as the y ordinate is followed, this is a very steep path indeed. Further investigation being deemed necessary, the limit cycles were recalculated and plotted as phase planes. An example is shown in Fig. 14. The stable steady solution is shown as a filled circle, while the "upper" unstable steady solution (the saddle) is

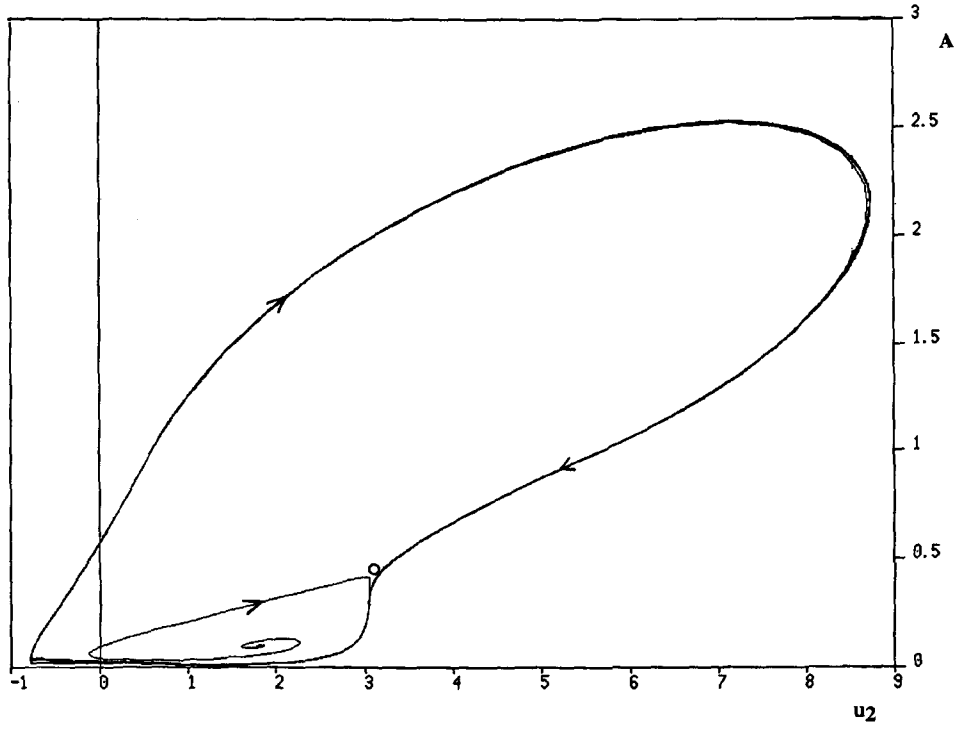

Figure 14. A (A, u_2) phase-plane plot of an integration for $p_u = 350$ and $p_e = 226.6$ started from the equilibrium point on the lower branch of the unstable steady solution path. This corresponds, for example, to a trajectory beginning just to the right of the homoclinic connection on the lower solution path of Fig. 9, panel K. The solution spirals out, approaches the saddle point (open circle) very closely and subsequently becomes a limit cycle with a large amplitude. The location of the stable equilibrium point (tube open) is shown as a filled circle.

shown as an open circle. The solution was started from the lower unstable steady solution (the repellor).

Examination of the plot shows the trajectory spiralling out until a close interaction occurs with the saddle point. The solution approaches the saddle with a fairly high speed and then almost stops there. The solution then recedes from the saddle point and the area of the tube drops almost to zero. The solution is subsequently driven into large-amplitude limit-cycle oscillations where the A^{-1} terms again drive the model close to an integrator "crash".

This limit cycle is fundamentally different from others encountered, in that its excursions reach a value greater than the value of the stable equilibrium (i.e. the tube-open condition). When this limit cycle was plotted while slowly reducing p_e, the system was seen to exhibit a blue-sky catastrophe; i.e. the limit cycle disappeared via a homoclinic connection. Thus, two fundamentally different homoclinic orbits have been identified (neither transverse) and are shown in panels hc1 and hc2 of Fig. 13.

Panel (viii) of Fig. 13 represents the topological behaviour of region (viii) which fits consistently with the behaviour in neighbouring regions. The osculatory point at $(p_u, p_e) \approx (324, 217)$ is thus a co-dimension-2 bifurcation point which links the topologies of regions (vi), (vi), (vii) and (viii).

The last schematic bifurcation diagrams shown in Figs. 9 and 11 were postulated for values of p_u to the far right of the (p_u, p_e)-space diagram, corresponding to regions J and K and regions IX and XI of Figs. 8 and 10, respectively. These sketches in each case show the connection point of the unsteady solution path moving toward the lower fold point, and at the same time becoming steep. (Such a path would look different, and perhaps more sensible, if the time-averaged value of a limit cycle were used as the y ordinate instead of the limit-cycle maximum value.) The main point to be made here is that the limit cycles grow to a large amplitude quickly as one follows the unsteady solution path away from the homoclinic connection. In fact, the limit cycles soon develop to the point where they are not followable with a Runge–Kutta integrator; the amplitude appears to grow without bound.

This explanation of the far right of (p_u, p_e) space is put forward as a suggestion rather than a rigorous explanation. The development of an explanation is hindered by the fact that the limit cycles which emanate from the homoclinic connection to the right of (p_u, p_e) space are very difficult to study. They exist in only a very small region (of either p_u or p_e) near the connection, outside which the oscillations tend to grow without bound.

Comparison with experiment. Comparison between the numerical analysis of the model and actual experimental results must be approached by

remembering that the model is of lumped-parameter type, while the physical situation could be more properly represented with partial differential equations. With this in mind, it is still possible to compare results in those parts of control space or with those sorts of behaviour which the model would be expected to represent well. The paper of Bertram *et al.* (1991) describes the flow through a thick-walled silicone rubber tube and discusses the transition between different types of behaviour in terms of bifurcation theory.

The two transitions discussed by Bertram *et al.* (1991) which show some similarity with experiment are the sudden and hysteretic jump from the upper stable steady equilibrium of (e.g.) Fig. 9, panel D (A close to one corresponding to an open tube), to the lower one (collapsed tube), and the suspected loss of limit-cycle oscillations through a homoclinic connection.

Bertram *et al.* (1991) suggest that the hysteretic transition between the collapsed and open tube states observed experimentally as p_e is increased can be represented by a pair of saddle-node bifurcations. This type of behaviour has been demonstrated explicitly in the analysis of the model here (see Fig. 9, panel D) and was also seen in an analysis of the model of Cancelli and Pedley (1985) by Jensen (1990).

The tube was also seen to vary abruptly between the open state and oscillations, with a degree of hysteresis, as p_e was varied. It was noted that period-lengthening was occasionally seen as p_e was decreased before the abrupt transition to the open tube state. This type of behaviour is quite similar to that near the homoclinic connections found in the analysis of the model (see Fig. 3). Bertram *et al.* (1991) suggested several possible topological configurations by which oscillations could disappear in this abrupt manner. Their task was made difficult by the fact that not all mathematically possible solutions are attainable experimentally. This is where the analysis of a model can lend valuable insight into the most likely configuration, and in this case a homoclinic connection seems quite feasible.

Bertram *et al.* (1991) also discuss the experimentally observed transition between low-frequency oscillations and high-frequency noise-like oscillations. This transition is observed to be either hysteretic or non-hysteretic and quasi-periodic during the transition. The proposed explanation for the transition is in terms of a four-dimensional manifold, and the specific topology describing the quasi-periodicity is a two-torus. This type of behaviour is not displayed by the model, since the dynamics are limited to two-dimensional non-toroidal manifolds.

It has been pointed out by Bertram and Pedley (1983) in a paper discussing the experimental separation of flow in an indented channel that the Strouhal number (for both theory and experiment) of the self-excited oscillations they investigated is somewhat greater than 1. This suggests that

the downstream head loss, found to be critical for oscillations, will not be quasi-steady (as assumed in the model discussed in this paper). It is interesting to speculate on the possibly richer dynamical system (increased in dimension by 1) which would result from the inclusion of a realistically unsteady term in the formula for downstream head loss.

Conclusions. The analysis of the model using the AUTO-86 package has resulted in a clear picture of its behaviour over the range of values studied for the two control parameters p_u and p_e. It should be remembered that only two out of a total of eight possible control parameters have been investigated, amounting to a two-dimensional slice in eight-dimensional control space. Although this is a sobering thought, remember that the two parameters studied here (p_u and p_e), along with R_1 and R_2, would be the first parameters likely to be varied in an experimental situation. This makes R_1 and R_2 strong candidates for further bifurcation studies.

The dynamical behaviour exhibited by the model proved to be of surprising variety and complexity, considering it was always recognised to be a simple and, in some ways, limited model capable of modelling only certain types of oscillations. In terms of its bifurcation behaviour, it has exhibited the two co-dimension-1 type bifurcations of a steady solution—the Hopf and the fold—and the cyclic fold which is a codimension-1 bifurcation of an unsteady solution. It has also exhibited a codimension-2 type bifurcation point—the Hopf-fold-homoclinic collision—and a global bifurcation in the form of the homoclinic connection responsible for the blue-sky catastrophe. An important point that arose from detailed consideration of this homoclinic connection is that the connection is not transverse. This fact precludes the model displaying some of the more complex behaviour associated with transverse homoclinic connections, such as homoclinic tangles and dynamical chaos (Guckenheimer and Holmes, 1986). Related to this observation is the fact that the model was found to display dynamical behaviour constrained to a two-dimensional centre manifold. This limits the kind of oscillatory behaviour possible to simple limit cycles (displayed by the model); no evidence was found of quasi-periodicity or mode locking (Thompson and Stewart, 1986).

In terms of the model's relationship to experimentally derived data, the detailed bifurcation analysis provided by AUTO has presented topological configurations with qualitatively similar bifurcation behaviour to that seen in experiment. This may help explain the topological changes responsible for the changes seen experimentally, particularly since some of the points in control space found here are difficult or impossible to find experimentally. The existence of a homoclinic connection is a good example. One can

"home-in" on such a point numerically, while experimentally other factors, such as noise and a lack of such infinite fine-tuning, serve to blur such a bifurcation point. This is important because, as seen in this analysis, the period lengthening associated with a homoclinic connection occurs only very close to the connection itself. It is thought that further refinement of the model will lead to a higher-dimension dynamical system and a possibly greatly enriched behaviour.

The authors would like to thank E. Doedel for use of the software package AUTO-86, P. Blennerhassett for advice on its installation and use, and M. Myerscough for useful discussions.

APPENDIX

The Model Equations. The lumped-parameter model under consideration is described by Bertram and Pedley (1982). A brief derivation of the then-proposed equations is given here. (Nomenclature is given in Table A1.) Twelve equations can be formed, using the basic laws of fluid mechanics, from the intrinsic assumptions of the model. These can then be reduced to an autonomous set of three ordinary differential equations.

The Basic Equations. The model consisted of a "Starling resistor" (an elastic tube mounted within a pressurised chamber) and its associated upstream and downstream

Table A1. Nomenclature

Symbol	Meaning
p_u	Constant pressure head
p_e	Chamber pressure
p_1	Upstream pressure
p_2	Downstream pressure
R_1	Upstream resistance
R_2	Downstream resistance
I_1	Upstream inertance
I_2	Downstream inertance
l	Length of collapsible section of tube
P_k	Constitutive constant
R_k	Resistance constant
p	Pressure at the point of maximal collapse
A_v	Average cross-sectional area of collapsed section of tube
u_1	Upstream fluid velocity
u_2	Downstream fluid velocity
A	Cross-sectional area at the point of maximal collapse
$P(A)$	Tube constitutive law
$f(A)$	Head-loss expression
$R(A)$	Shape-dependent Poiseuille resistance per unit length

conduits (Fig. 1). A variable resistance is situated in both the upstream and downstream conduits. The upstream and downstream conduit inertances can also be changed, although with more difficulty.

The system variables are normalised with respect to the uncollapsed cross-sectional radius $\hat{r}_0$, a fluid velocity $\hat{u}_0$ and the fluid density ρ. Thus,

pressure $$\hat{p}_0 = \rho \hat{u}_0^2,$$

flow rate $$\hat{Q}_0 = \hat{u}_0 \hat{A}_0,$$

area $$\hat{A}_0 = \pi \hat{r}_0^2,$$

resistance $$\hat{R}_0 = \frac{\rho \hat{u}_0}{\pi \hat{r}_0^2},$$

inertance $$\hat{I}_0 = \frac{\rho \hat{r}_0}{\hat{A}_0}$$

and

$$A = \frac{\hat{A}}{\hat{A}_0},$$

etc.

Mass Conservation. The first of the 12 basic equations is formed from the laws of mass conservation. First, an approximate average area of the collapsed section of the tube is denoted A_v, where

$$A_v = \tfrac{1}{2}(1 + A). \tag{A1}$$

An approximate average velocity within the collapsed section of the tube can also be defined by

$$u_v A_v = \tfrac{1}{2}(u_1 + u_2). \tag{A2}$$

The volume of fluid which is accumulating in the collapsed section of the tube over time relates to the flows in and out of this section as

$$u_1 - uA = l\dot{A}_v, \tag{A3}$$

where the overdot denotes differentiation with respect to time.

Downstream, mass conservation gives the simple relation

$$u_2 - uA = 0. \tag{A4}$$

The Inlet and Outlet Pipes. The Reynolds number of the flow is assumed low enough that the flow will be laminar. This means that the flow in the inlet pipe can be characterised by

$$p_u - p_1 = R_1 u_1 + I_1 \dot{u}_1; \tag{A5}$$

similarly, downstream

$$p_2 = R_2 u_2 + I_2 \dot{u}_2. \tag{A6}$$

Energy in the Upstream Section of the Collapsed Tube. Within the collapsed section of the tube the energy loss due to viscous resistance and accumulation of inertia must be considered. The former is assumed to be concentrated in the last quarter of the collapsible segment and is calculated using the resistance function $R(A)$. This function represents the Poiseuille resistance per unit length for the tube when circular ($A \geq 1$) and approximately when elliptical ($A < 1$). Therefore, in the collapsed section of the tube upstream of the constriction,

$$p_1 + \tfrac{1}{2}u_1^2 - (p + \tfrac{1}{2}u^2) = \tfrac{1}{4}lR(A)u + l\dot{u}_v, \tag{A7}$$

where

$$R(A) = \begin{cases} \dfrac{2R_k}{A}, & \text{for } A \geq 1, \\ R_k\left(1 + \dfrac{1}{A^2}\right), & \text{for } A < 1, \end{cases} \tag{A8}$$

and

$$R_k = \frac{4\mu}{\rho \hat{u}_0 \hat{r}_0}. \tag{A9}$$

Momentum in the Downstream Section of the Collapsed Tube. Downstream of the constriction, the fluid is assumed to emerge as a separated jet, resulting in energy dissipation and hence less than full pressure recovery. The equation proposed to describe this situation is that for quasi-steady jet head loss, obtained by applying a momentum balance at the constriction. Bertram and Pedley (1982) point out that the flow here is likely to be and indeed was found to be unsteady (i.e. the Strouhal number is substantial). Thus this is a possible source of error in the model predictions. The momentum equation for the constriction is then

$$p - p_2 = -f(A)u_2^2, \tag{A10}$$

where

$$f(A) = \begin{cases} \dfrac{1}{A} - 1, & \text{for } A < 1, \\ \dfrac{1}{2}\left(\dfrac{1}{A^2} - 1\right), & \text{for } A \geq 1 \text{ or } u_2 < 0. \end{cases} \tag{A11}$$

The latter form of $f(A)$, applied for a distended tube or reversed flow, yields Bernoulli's equation.

Elastic Behaviour of the Tube. The collapsible-tube constitutive law used describes the elastic behaviour of the tube wall in response to the transmural pressure applied to it. Bertram and Pedley (1982) made the gross assumptions (1) that the area of the collapsible segment could be completely specified by the area at the narrowest point (A) and (2) that this area could be related solely to the transmural pressure at this point. Therefore,

$$p - p_e = P(A), \tag{A12}$$

where the authors chose to use a slight modification of a constitutive relationship, developed by Shapiro (1977), which is based on static experiments using thin-walled rubber tubes and which ignores longitudinal tension:

$$P(A) = \begin{cases} P_k(1 - A^{-3/2}), & \text{for } A < 1, \\ 100P_k(A - 1), & \text{for } A \geq 1. \end{cases} \tag{A13}$$

Reduction of the equations. The above 12 equations are reduced to a set of three autonomous differential equations of the form

$$\dot{A} = f(\text{free parameters}, A, u_1, u_2),$$

$$\dot{u}_1 = f(\text{free parameters}, A, u_1, u_2),$$

$$\dot{u}_2 = f(\text{free parameters}, A, u_1, u_2).$$

Area of the constriction.

$$\dot{A} = \frac{2(u_1 - u_2)}{l}. \tag{A14}$$

Downstream fluid velocity.

$$\dot{u}_2 = \frac{P(A) + p_e + f(A)u_2^2 - R_2 u_2}{I_2}. \tag{A15}$$

Table A2. Non-dimensional values used originally (Bertram and Pedley, 1982)

Constant	Value
R_2	50, 75, 150
I_2	25
r	0.5, 1.5
R_1	25, 37.5, 75; 75, 113, 225
I_1	12.5, 37.5
p_e	200
p_u	295
l	10
R_k	0.00466
P_k	4

Upstream fluid velocity.

$$\dot{u}_1 = \left[\frac{A+1}{l+(A+1)I_1}\right]\left[p_u - P(A) - p_e - R_1 u_1 + \frac{1}{2}u_1^2 - \frac{u_2^2}{2A^2} - \frac{lR(A)u_2}{4A} + \frac{2(u_1^2-u_2^2)}{A^2+2A+1} - \frac{l\dot{u}_2}{A+1}\right]. \tag{A16}$$

Thus, a set of three ordinary differential equations in a suitable form for numerical solution—(14), (15) and (16)—has been derived.

Values Used for the Free Parameters. Bertram and Pedley (1982) chose to examine three sets of input data, corresponding to three different values of R_2. In each case, the other parameters were kept constant. An added simplification was made by making both the upstream conduit resistance and inertance related to their downstream equivalents by a factor r. The dimensionless parameters which were used are listed in Table A2.

It is of interest to consider some real physical dimensions, based on the paper of Conrad (1969), in relation to test rigs used by Bertram and Pedley since their 1982 paper. For example, a typical value of 6.35 mm for r_0 and an arbitrarily chosen value of 0.15 m s^{-1} for u_0 result in the values $\hat{p}_e = 4.5$ kPa, $\hat{p}_{u_1} = 6.6$ kPa, $\hat{l} = 63.5$ mm, $\hat{P}_k = 90$ Pa, $\hat{R}_1 = 44.4 \times 10^6$ kg m^{-4} s^{-1}, $\hat{R}_2 = 88.8 \times 10^6$ kg m^{-4} s^{-1}, $\hat{I}_1 = 0.63 \times 10^6$ kg m^{-4} and $\hat{I}_2 = 1.25 \times 10^6$ kg m^{-4}.

REFERENCES

Abraham, R. H. and C. D. Shaw. 1984. *Dynamics—The Geometry of Behaviour. Part Two: Chaotic Behaviour*. Santa Cruz, California: Aerial Press.

Bertram, C. D. and T. J. Pedley. 1982. A mathematical model of unsteady collapsible tube behaviour. *J. Biomech.* **15**, 39–50.

Bertram, C. D. and T. J. Pedley. 1983. Steady and unsteady separation in an approximately two-dimensional indented channel. *J. Fluid Mech.* **130**, 315–345.

Bertram, C. D., C. J. Raymond and T. J. Pedley. 1990. Mapping of instabilities for flow through collapsed tubes of differing length. *J. Fluids and Structures* **4**, 125–153.

Bertram, C. D., C. J. Raymond and T. J. Pedley. 1991. Application of nonlinear dynamics concepts to the analysis of self-excited oscillations of a collapsible tube conveying a fluid. *J. Fluids and Structures* **5**, 391–426.

Cancelli, C. and T. J. Pedley. 1985. A separated-flow model for collapsible tube oscillations. *J. Fluid Mech.* **157**, 375–404.

Conrad, W. A. 1969. Pressure–flow relationships in collapsible tubes. *IEEE Trans. Biomed. Engng.* **16**, 284–295.

Doedel, E. and J. P. Kernévez. 1986. AUTO: Software for continuation and bifurcation problems in ordinary differential equations. Applied Mathematics Report, California Institute of Technology.

Grotberg, J. B. and N. Gavriely. 1989. Flutter in collapsible tubes: a theoretical model of wheezes. *J. Appl. Physiol.* **66**, 2262–2273.

Guckenheimer, J. and P. Holmes. 1986. *Nonlinear Oscillations, Dynamical Systems and Bifurcations of Vector Fields*. New York: Springer-Verlag.

Guyton, A. C. 1986. *A Textbook of Medical Physiology*. Philadelphia: Saunders.

Jensen, O. E. 1990. Instabilities of flow in a collapsed tube. Appendix A: hysteresis of the steady solutions. *J. Fluid Mech.* **220**, 623–659.

Kamm, R. D. and T. J. Pedley. 1989. Flow in collapsible tubes: a brief review. *ASME J. Biomech. Engng.* **111**, 177–179.

King, A. S. and J. McLelland. 1984. BIRDS their structure and function. London: Ballière Tindall and Cox.

Knowlton, F. P. and E. H. Starling. 1912. The influence of variations in temperature and blood-pressure on the performance of the isolated mammalian heart. *J. Physiol.* **44**, 206–219.

Matsuzaki, Y. 1986. Self-excited oscillation of a collapsible tube conveying a flow. In *Frontiers in Biomechanics*. G. W. Schmid-Schonbein, S. L-Y. Woo and B. W. Zweifach (Eds). New York: Springer-Verlag.

Morgan, P. and K. H. Parker. 1989. A mathematical model of flow through a collapsible tube. I. Model and steady flow results. *J. Biomech.* **22**, 1263–1270.

Shapiro, A. H. 1977. Steady flow in collapsible tubes. *ASME J. Biomech. Engng.* **99**, 126–147.

Thompson, J. M. T. and H. B. Stewart. 1986. *Nonlinear Dynamics and Chaos: Geometrical Methods for Engineers and Scientists*. Chichester: Wiley.

Ur, A. and M. Gordon. 1970. Origin of Korotkoff sounds. *Am. J. Physiol.* **218**, 524–529.

Received 8 February 1995
Accepted 6 August 1995